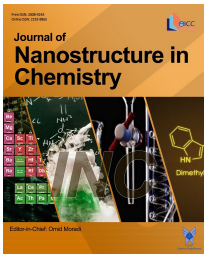

Volume 15, Issue 5, 152520 (1-15)

Journal of Nanostructure in Chemistry (JNSC)

https://doi.org/10.57647/jnsc.2025.1505.20

Catalytic and Antibacterial Activities with Molecular Docking Analysis of Chitosan and Polyethylene Glycol-NiO_2 Nanostructures

Muhammad Imran[1], Iram Shahzadi[2], Ali Haider[3], Mudassir Hassan[4], Anwar Ul-Hamid[5], Waseem Safdar[6], Junaid Haider[6], Muhammad Ikram[4,*]

[1]*Interdisciplinary Research Center for Hydrogen Technologies and Carbon Management (IRC-HTCM), King Fahd University of Petroleum & Minerals, Dhahran 31261, Saudi Arabia.*
[2]*School of Pharmacy, University of Management and Technology, Lahore 54770, Pakistan.*
[3]*Department of Clinical Sciences, Faculty of Veterinary and Animal Sciences, Muhammad Nawaz Shareef, University of Agriculture, Multan 66000, Punjab, Pakistan.*
[4]*Solar Cell Applications Research Lab, Department of Physics, Government College University Lahore, Lahore 54000, Punjab, Pakistan.*
[5]*Core Research Facilities, Research Institute, King Fahd University of Petroleum & Minerals, Dhahran 31261, Saudi Arabia.*
[6]*Department of Biological Sciences, National University of Medical Sciences, Rawalpindi 46000, Pakistan.*

[*]**Corresponding author:** dr.muhammadikram@gcu.edu.pk

Original Research

Received:
11 August 2025
Revised:
9 September 2025
Accepted:
19 September 2025
Published online:
17 October 2025

Abstract:

Toxic dyes and microbes in water have an alarming effect on the integrity of the environment and dairy industries. In this study, 2 and 4 wt.% of chitosan (CS) and 3% of polyethylene glycol (PEG) were incorporated to nickel oxide (NiO_2) nanostructures (NSs) to degrade dyes and to kill bacteria effectively, synthesized via the low-temperature co-precipitation technique. The motive of the research is to enhance catalytic and antimicrobial properties through surface modification and the generation of more active sites upon incorporation of dopants. X-ray crystallographic patterns confirm the hexagonal crystal structure of NiO_2 and a reduction in crystallite size with doping. The band gap energy of NiO_2 increases from 3.17 to 3.25 eV upon doping. TEM elucidates the formation of an interconnected network of nanorods and nanoparticles with reduced agglomeration upon PEG and CS addition. Doping controlled the morphology and charge recombination dynamics of NiO_2, which significantly boosts the catalytic and antibacterial potential. Particle size of the NiO_2 nanostructures decreases from 34.7 to 24.53 nm with the addition of dopants. Notably, the highly doped sample exhibited maximum RhB degradation of 92.3% in neutral medium and maximum inhibition zone of 5.25 ± 0.03 mm against gram-negative multiple drug-resistant *Escherichia coli* (MDR *E. coli*) ($p < 0.05$). The computational results correspond with observational data, providing compelling support for the microbial efficacy of CS/PEG-NiO_2 in suppressing DNA gyrase.

Keywords: Chitosan; Antimicrobial; Dye degradation; Nanostructures

Cite this article: Imran, M., Shahzadi, I., Haider, A., Hassan, M., Ul-Hamid, A., Safdar, W., Haider, J., Ikram, M. Catalytic and Antibacterial Activities with Molecular Docking Analysis of Chitosan and Polyethylene Glycol-NiO_2 Nanostructures. *J Nanostruct Chem* **15**(5), 152520 (2025).

1. Introduction

Water is the primary requirement, enabling human activity to develop and people to work [1]. However, more than 150 million people lack access to fresh water. With rapid industrialization and economic activities, water is being contaminated by directly discharging numerous waste products like plastic, pesticides, dyes, organic and inorganic contaminants, endangering aquatic life [2, 3]. Dyes are excessively utilized in several industries such as cosmetics, paper, tex-

tiles, pharmaceuticals and rubber [4]. Among these sectors, the textile industry is the biggest user of dyes and pigments, producing most pollutants. Rhodamine B (RhB) is a water-soluble, highly stable, toxic, non-biodegradable synthetic dye. RhB is utilized to make stamp pad ink, dye lasers, ball pens and crackers. RhB's extensive use causes skin, gastrointestinal, eye infections and damages thyroid and liver [5, 6]. In recent years, it has been challenging to degrade dye because of high water solubility and diverse structures [7]. Traditional water treating processes such as ion exchange, adsorption, chemical precipitation and membrane filtration have been implemented to remediate contaminated water [8, 9]. Unfortunately, these techniques have several problems such as large-scale cost, immersed energy consumption, and derived pollution from deficient dye removal and transfer [10]. Among all techniques, catalytic dye degradation in the presence of nanomaterials has been preferred because of less time to degrade dyes, less toxic byproducts, and environmentally friendly [11].

Nanomaterials (NMs) can degrade dyes effectively, ascribed to distinct properties like low toxicity, high stability in different conditions, and a large surface area suitable for catalysis and enhances their interaction with bacteria. Their controlled size, shape, and large surface-to-volume ratio make them promising for several environmental applications [12–14]. Metal oxides (MO) are widely used in environmental remediation owing to their versatility in synthesis [15]. Among them, nickel oxide (NiO_2) is cheap, accessible and electrochemically stable, has gained the attention of researchers owing to its optical, mechanical, electronic and magnetic properties, and is frequently used in fuel cell electrodes and catalysis [16, 17]. NiO_2 is a typical p-type semiconducting material, possessing a wide band gap energy ($3.6 - 4$ eV) and providing properties of enhanced biocompatibility, excellent reactivity, stability, durability, and outstanding bacterial resistivity [18, 19]. Ahmed et al. synthesized NiO nanosheets modified with gold particles that provide greater surface area for the improved electrocatalytic activity [20]. Nickel-based nanomaterials provide features of stability, selectivity and a highly reproducible fabrication process [21]. NiO NPs demonstrated excellent bactericidal behavior against Gram-positive strain of bacteria owing to strong charge transfer capability [22, 23]. In general, NiO_2 has insufficient surface area, is highly unstable and agglomerates very quickly without capping agents [24, 25]. To overcome these problems, polymers such as, polyethylene glycol (PEG), starch (St), polyacrylic acid (PAA) and chitosan (CS) have been used as a capping agent. Polymer-based composites garnered significant interest attributed to their environmental sustainability, biocompatibility, and biodegradability [26]. Polyethylene glycol (PEG) is water-soluble, less toxic, and has good biocompatibility, which makes it suitable as a capping agent [27]. PEG can reduce agglomeration, control shape and size of nanoparticles by binding nanoparticle surfaces through hydrophobic or electrostatic interaction [25]. Chitosan-based materials emerged as a promising candidate for a wide range of applications owing to its biocompatible and low-toxic nature. It exhibits exceptional antibacterial properties against ascribed to its cationic nature against which compromises the membrane integrity by enabling interactions with proteins and lipids (negatively charged), leading to cell damage [28, 29]. Furthermore, chitosan (CS) is a polysaccharide with high molecular weight and the second most abundant polymer. CS has a remarkable ability to remove contaminants from water due to its highly reactive amino and hydroxyl groups through chemical modification, which leads to better catalytic and bactericidal activity [30]. Here, we used a facile, green, and low-cost co-precipitation method to prepare NiO_2 and CS/PEG doped NiO_2 nanostructure (NSs).

The study aims to investigate optical, morphological, and structural properties of NiO_2, (3 wt.%) PEG-doped NiO_2 and (2 and 4 wt.%) CS doped PEG-NiO_2 prepared through a co-precipitation approach. Dual polymers aided in restricting the agglomeration of NiO_2 nanoparticles, which served to control their dimensional growth and enabled the enhancement in surface area for the excellent catalytic and antibacterial activities. Moreover, the synthesized nanocatalyst dye degradation potency against RhB and bactericidal efficacy for MDR *E. coli* were tested.

2. Experimental

2.1 Materials

Nickel nitrate ($Ni(NO_3)_2 \cdot 6H_2O$), polyethylene glycol [$(C_2H_4O)_n{\cdot}H_2O$] were purchased from Fluka Chemika, NaOH (99%) and chitosan $(C_6H_{11}NO_4)_n$ were procured from Sigma-Aldrich (Germany).

2.2 Synthesis of NiO_2 and CS/PEG doped NiO_2

Co-precipitation method was used to synthesize NiO_2 nanoparticles. Initially, 0.2 M solution of Ni $(NO_3)_2 \cdot 6H_2O$ was prepared in deionized water (DI water) under constant stirring and heating at 85 °C for 30 minutes. Afterward, a suitable amount of NaOH was poured to maintain $\sim$ pH 8 and to obtain precipitates. Colloidal solution was centrifuged at 8000 rpm for 8 minutes twice to remove impurities and heated overnight at 130 °C for drying. To acquire fine powder, the synthesized material was crushed with a mortar and pestle after cooling. Similarly, to prepare PEG-NiO_2 (3 wt.%) of PEG was added to the above solution (sample 2). For CS/PEG-NiO_2, various concentrations (2 and 4 wt.%) of chitosan were incorporated into PEG-NiO_2 through the same method. The synthesis process of the prepared sample is illustrated in Fig. 1.

2.3 Catalytic activity (CA)

RhB was chosen as an organic pollutant to examine the catalytic activity of NiO_2, PEG-NiO_2 and CS/PEG-NiO_2 in the presence of $NaBH_4$ (reducing agent) under dark conditions. Initially, 400 µL from 0.1 M $NaBH_4$ solution was mixed with RhB solution (3 mL) followed by integration of NiO_2 and CS/PEG doped NiO_2 solution (400 µL). Nanocatalyst increases rate of by decreasing the activation energy. Disappearance of RhB color (pink), confirmed degradation of RhB into leuco-rhodamine B (LRhB) and absorption spectrum was observed with UV-Vis spectroscopy.

Degradation of dye was noticed in acidic, basic and neutral

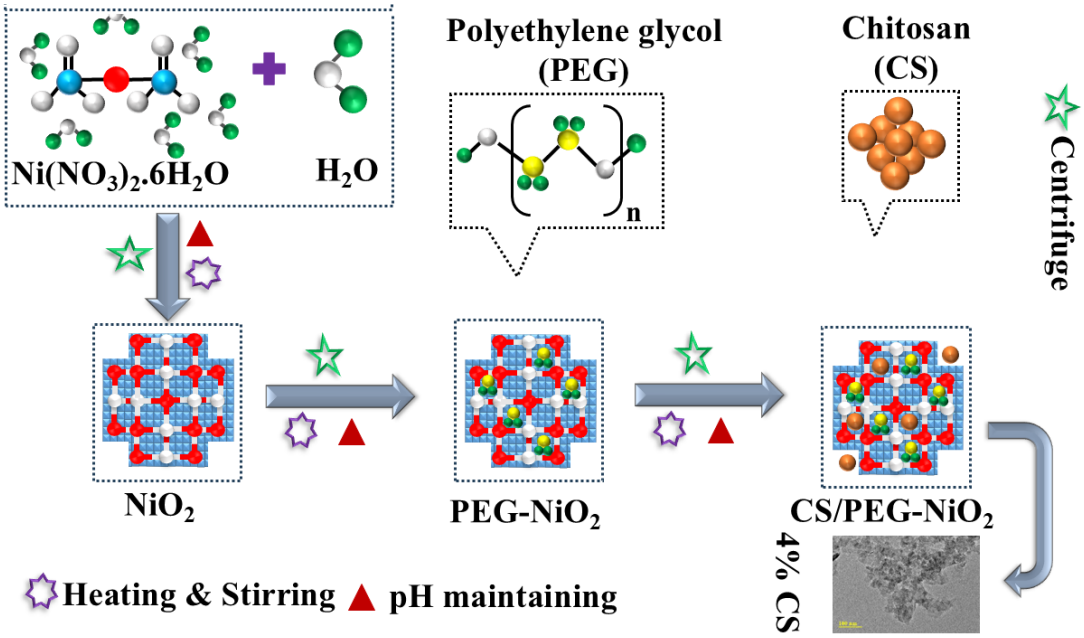

Figure 1. Schematic representation of the synthesis of NiO_2 and CS/PEG-doped NiO_2.

media and degradation % was calculated by equation (2).

$$\text{Degradation}\% = \frac{C_0 - C_t}{C_0} \times 100 \quad (1)$$

where, C_0 = initial and C_t = final concentration of RhB after a specific time. Statistical reliability of the catalytic activity was ensured by performing the experiments in triplicate ($n = 3$).

2.4 Catalytic mechanism

Incorporation of reducing agent ($NaBH_4$) and prepared the nanocatalyst in RhB solution is essential for catalytic dye degradation. $NaBH_4$ functions as a reducing agent, donates an e^-, which is accepted by RhB that serving as an oxidizing agent, respectively converts RhB into leuco RhB. In contrast, the huge energy barrier between reacting species hinders the reaction kinetics, making degradation a time-consuming process. However, the addition of NCs (NiO_2 and doped NiO_2) accelerates the reaction kinetics, enabling the transfer of electrons from the donor to the acceptor, resulting in the reduction of RhB. The NCs accelerate the reaction kinetics and boost the degradation rate by lowering the kinetic barrier. Firstly, $NaBH_4$ dissociates into Na^+ and BH_4^- that adsorbed onto the surface of NCs through an adsorption process. These ions release electrons to the catalyst and split into H^+ ions, NCs serve as an electron relay system by transferring electrons from BH_4^- to RhB. The H^+ ions attacked RhB, resulting in the decolorization of dye due to the breakdown of π bond of RhB (Supplementary Fig. 1) [31, 32]. The amount of catalyst utilized during a reaction is critical since the reduction of dye directly relates to the amount of catalyst.

2.5 Isolation and identification of MDR *E. coli*

2.5.1 Sample collection

Through direct milking into sterile glassware, raw milk samples were collected from clinical mastitis positive lactating cows at various veterinary hospitals, farms and markets in Pakistan. Obtained raw milk specimens were immediately delivered to laboratory at 4 °C. *Escherichia coli* (*E. coli*) isolation and purification in raw milk was enumerated on MacConkey agar in triplicates, and all plates were observed for bacteria growth after aerobic incubation at 37 °C for 48 h.

2.5.2 Characterization and identification of bacterial isolates

The initial identification of isolated *E. coli* was based on morphological structures of colonies determined by Gram's staining and biochemical characterization proceeded using biochemical tests considering National Committee for Clinical Laboratory Standards (NCCLS) guidelines [33]. The antibiotic susceptibility by disk diffusion method was concluded by swabbing 0.5 MacFarland standard growths of isolated *E. coli* with application of antibiotic disks following aerobic incubation of petri dishes at 37 °C for 24 hours. Bacteria depicted as resistant against at least three antibiotics were classified as multiple drug resistant (MDR) [34].

2.5.3 Antimicrobial activity

Overall, upon ten representative isolates of MDR *E. coli* obtained from mastitis milk the in vitro bactericidal potential of NiO_2, PEG-NiO_2 and CS/PEG-NiO_2 were elucidated by agar well diffusion method. 1.5×10^8 CFU/mL (0.5 McFarland standard) of MDR *E. coli* was swabbed on MacConkey agar plates. Sterile crock borer was used to generate wells of 6 mm diameter. NiO_2, PEG-NiO_2 and CS/PEG-NiO_2 were used at high (1.0 mg/50 µL) and low (0.5 mg/50 µL) concentrations. DI water 50 µL (negative control) and ciprofloxacin 0.005 mg/50 µL (positive control) were used. After loading of undoped and doped NiO_2 the petri dishes were incubated aerobically at 37 °C for 24 hours and obtained inhibition

regions were quantified using vernier caliper [35].

2.5.4 Statistical analysis

The inhibition zone diameters were examined statistically by one-way analysis of variance (ANOVA) using SPSS 24.0 to evaluate the bactericidal potential of undoped and doped NiO_2 considering $p < 0.05$ [36].

2.6 Structures preparation and docking studies

The three-dimensional structure of CS/PEG-NiO_2 was constructed utilizing Sybyl X2.0/SKETCH [37]. The synthesized CS/PEG-NiO_2 was subjected to energy optimization through the application of Tripos force field and Gasteiger Hückel atomic charges, facilitating a conformation that promotes biological activity. The protein structures underwent refining using structural preparation techniques in the SYBYL-X 2.0 module, including missing hydrogen atoms and applying electrical charges. The binding site was executed through the ligand-based protomol generation method, employing a protomol threshold of 0.50. The energy reduction procedure was executed using the Powell method, achieving a convergence gradient of 0.05 kcal $(mol)^{-1}$ over 1000 cycles. In conclusion, the Surflex-Dock module of the SYBYL-X 2.0 program was used to precisely place the energy-optimized nanostructure inside the active site of the 6L01 protein, which was then evaluated for binding interactions with their respective targets [38]. A minimum of ten optimal docked poses for each ligand-receptor complex were produced, utilizing the standard SYBYL grid parameters, with grid box dimensions automatically set to accommodate the binding cavity of 6L01. The Hammerhead scoring approach was used to evaluate these prospective ligand conformations.

3. Results and discussion

3.1 Physicochemical characterizations

Crystal structure, lattice planes, phase purity, cystallinity, and crystallite size of NiO_2 and CS/PEG doped NiO_2 was evaluated by XRD analysis (Fig. 2 (a)). Diffraction peaks observed at 33.10°, 38.59°, 52.1°, 59.17°, 62.8°, and 69.4° analogs to lattice plane (010), (011), (012), (110), (111), and (020) revealed the hexagonal structure of NiO_2 well synchronized with JCPDS card No. 96-901-1315. A minor diffraction peak at 31.90° (002) corresponds to another phase of nickel oxide (Ni_2O_3) having a hexagonal structure (JCPDS card No. 00-014-0481). With PEG, no extra peak was observed, ascribed to the low concentration of dopants and PEG acted as a modulator for crystal growth, leading to more intense peaks. Complexation, miscibility and interaction between CS and PEG disrupted regular arrangements of crystal lattice, resulting in disappearance of few peaks [39]. Average crystallite size calculated from Scherrer equation was found to be 39.03 nm for NiO_2, which decreases up to 18.16 nm with dopants. Furthermore, crystallinity of NiO_2 increases from 73 to 77% with increasing concentrations of dopants. Cumulative effect of polymers on the crystallinity of materials is in-lined with literature [40, 41]. The polycrystalline nature of NiO_2 and 4% CS/PEG-NiO_2 was confirmed through SAED analysis as shown in Fig. 2 (b-c), respectively.

The presence of functional groups and vibrational modes in NiO_2 and CS/PEG-doped NiO_2 were examined through FTIR spectroscopy (Fig. 3 (a)). Stretching vibrations of Ni-O witnessed by a broad transmittance band in $400-850$ cm^{-1} range and at 993 cm^{-1}, indicating the successful formation of NiO_2 [42]. C-H in plane bending vibrations appeared at 1045 cm^{-1} and CO_2 existence was confirmed by the presence of band at 2352 cm^{-1} [43]. Transmittance

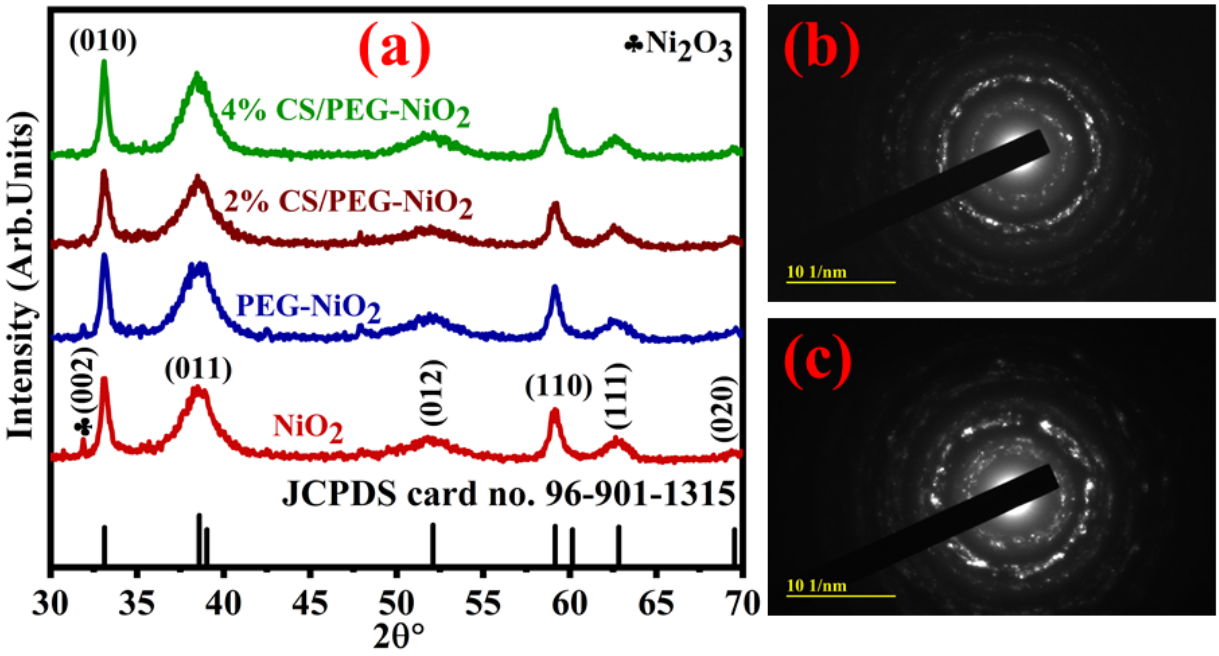

Figure 2. (a) XRD analysis of undoped and doped NiO_2 within $2\theta°$ ranging $30-70°$ (b-c) SAED diffraction patterns of NiO_2 and 4% CS/PEG-NiO_2, respectively

bands at 1653, 3651 and 1392 cm^{-1} were assigned to the fundamental H-O-H bending, O-H stretching vibrations of water molecules absorbed on the surface of the nanocatalyst and CO_3^{-2} vibrations, respectively [43, 44]. In PEG-NiO_2, PEG characteristic transmittance band was observed at 2850 cm^{-1} belonging to vibration of CH group [45]. With CS, bands intensity decreased gradually with increased CS concentration. In the FTIR spectrum of PEG-doped NiO_2, signal at 3400 cm^{-1} is associated with the attached hydroxyl group [46]. No additional band found in the spectrum of chitosan doped PEG-NiO_2 samples, although intensity of characteristics bands of PEG changed. This implies that CS and PEG have a unique kind of interaction resulted from the newly formed intermolecular hydrogen bonds between the two molecules [47].

An electronic transition spectrophotometer was employed to elucidate optical properties of NiO_2, PEG-NiO_2, and CS/PEG-NiO_2 (Fig. 3 (b)). NiO_2 showed absorption in the $245 - 780$ nm range, with typical absorption peaks around 300, 395, and 655 nm. Abrupt change in absorption around 385 ascribed to presence of NiO nanoparticles [48]. Higher intensity of peaks encouraged high yield of as-synthesized nanoparticles, while sharpness of peaks suggests that NiO_2 nanoparticles were stable [49]. Upon PEG, absorption increased with decreasing wavelength. Addition of CS into PEG-NiO_2, absorption enhanced gradually, resulting in enhancement of band gap energy (E_g). Tauc plot equation was used to calculate E_g of NiO_2 and CS/PEG-doped NiO_2 (Supplementary Fig. 2 (a-d)), found to be 3.17 eV which increased with dopant to 3.25 eV and well matched with reported E_g of nickel oxide [50].

TEM analysis was utilized to investigate internal morphology of NiO_2 and CS/PEG-doped NiO_2 (Fig. 4 (a-d)). NiO_2 showed non-uniform agglomerated nanoparticles with few nanorods on surface that may interact with nanoparticles (Fig. 4 (a)). Addition of PEG (capping agent) to NiO_2, PEG reduced size of nanostructures under effect of capping. Furthermore, more nanorods appear on surface of nanoparticles (Fig. 4 (b)). With lower concentration of CS, nanorods and nanoparticles were interconnected to form a network and it is difficult to identify the morphology of CS (Fig. 4 (c)). Agglomeration reduced slightly with higher concentration of CS (Fig. 4 (d)). Particle size of the NiO_2 nanostructures decreases from 34.7 to 24.53 nm with the addition of dopants and size distribution histograms extracted from TEM images are displayed in Supplementary Fig. 3.

Elemental composition of NiO_2 and CS/PEG-doped NiO_2 was ascertained using EDS analysis (Fig. 5 (a-d)). Purity and existence of NiO_2 were affirmed by strong Ni and O peaks in all synthesized materials. Incorporation of PEG and CS, new carbon peak appeared in doped samples ascribed to the presence of C in the dopants structure, confirming the doping of PEG and CS in NiO_2. Moreover, Au peaks appeared because of the coating on the samples during characterization to reduce charging effect.

Elemental distribution of highly doped material was investigated through EDS mapping analysis and represented with distinct colors (Supplementary Fig. 4 (a-d)). Different color images demonstrated presence of Ni, O, C in CS/PEG-NiO_2.

3.2 Catalytic degradation of dye

Catalytic potency of NiO_2 and CS/PEG doped NiO_2 was examined against RhB dye, with electronic transition spectroscopy in acid, basic and neutral media in Fig. 6, respectively. NiO_2, PEG-NiO_2, and (2 and 4%) CS/PEG-doped NiO_2 showed 80.25, 81.71, 83 and 86.71% degradation efficacy in acidic, 86.14, 86, 86.71 and 89.14% in basic and 90.55, 91.2, 91.4, and 92.3% in neutral medium, respectively (Fig. 6 (a-d)). Crystallite size, pH, shape, amount and surface area of the catalyst plays vital role in degrading dyes. As evident from XRD analysis, the crystallite size decreases which consequently increases the surface to volume ratio thereby enhancing degradation efficiency. Moreover, the formation of an interconnected network of NPs and NRs with chitosan addition facilitates the mobility of charge carriers that significantly impacts the degradation potential of prepared NCs. Maximum degradation was noticed in neutral medium, evolved to existence of RhB dye in different form (cationic and zwitter) in water and

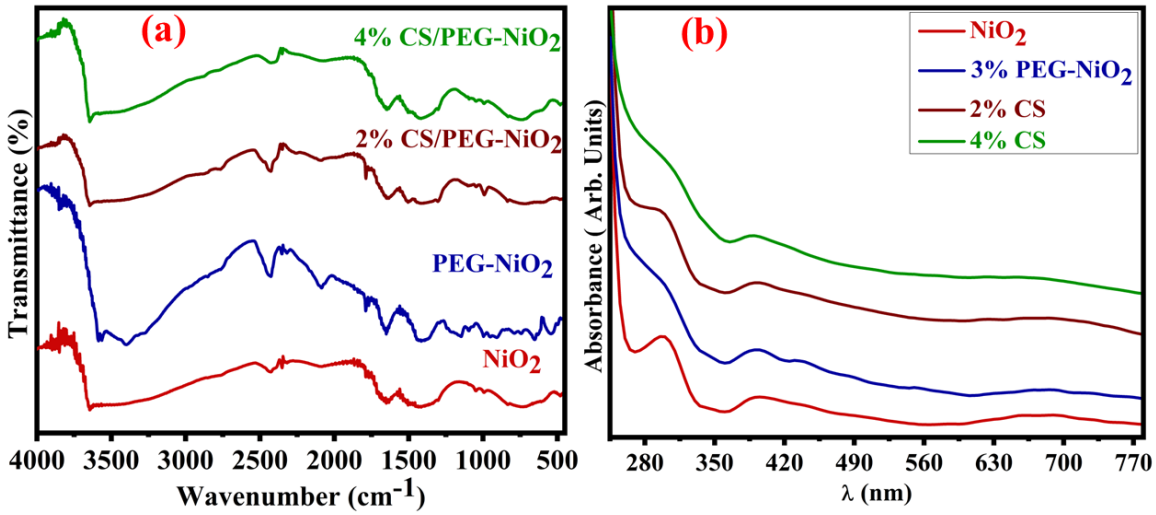

Figure 3. (a) FTIR spectra acquired in the wavenumber of $4000 - 450$ cm^{-1} (b) Electronic spectra of NiO_2 and doped NiO_2.

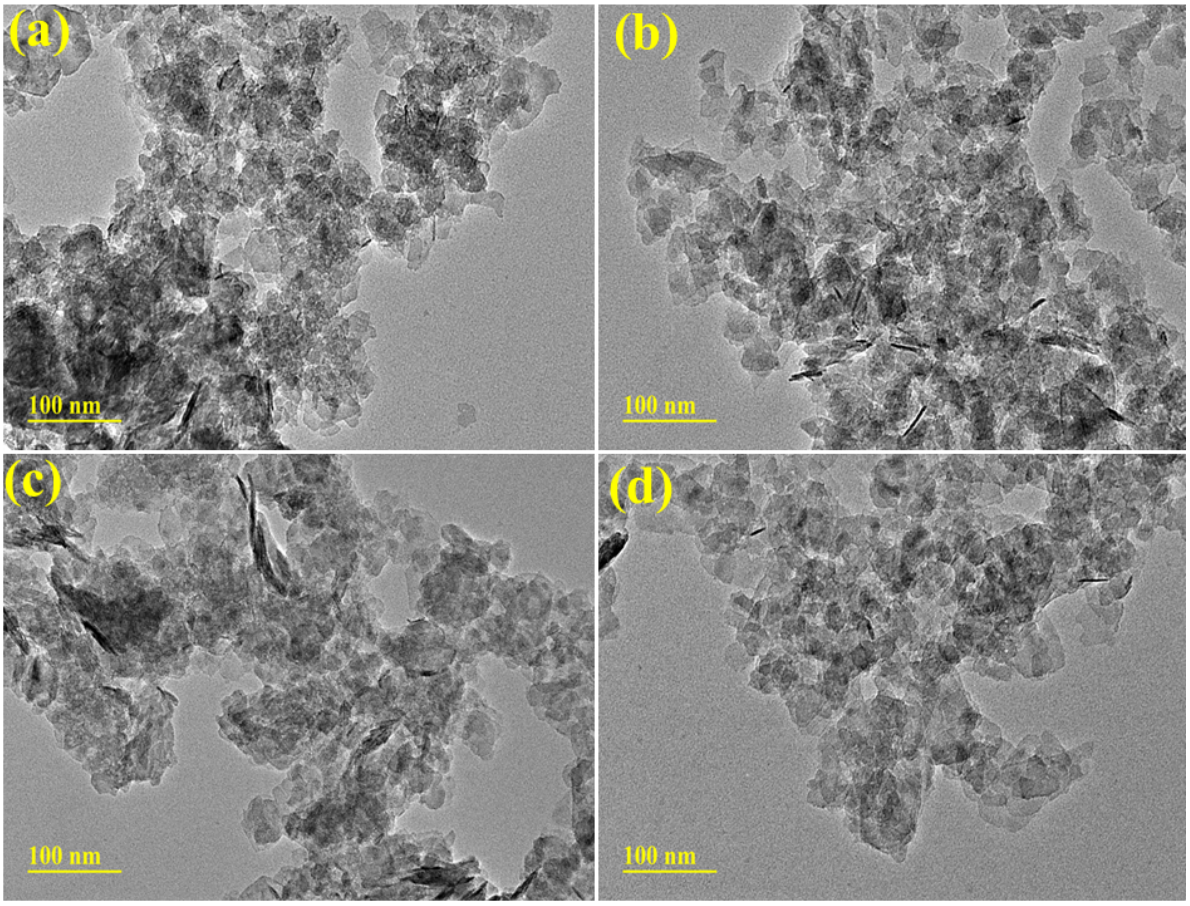

Figure 4. TEM images having resolution of 100 nm (a) NiO_2 (b) 3% PEG-NiO_2 (c-d) 2 and 4% CS/PEG-NiO_2.

active sites generated on the surface of the nanocatalyst. Lowest degradation of RhB was observed in acidic medium because of H^+ ions produced in solution got neutralized by OH^-, while intermediate degradation was seen in neutral medium. A key aspect in designing an ecologically sustainable nanocatalyst is the effective recovery and recycling after the catalytic activity. Under optimal conditions, six cycles were conducted to evaluate the reusability of 4% CS/PEG-doped NiO_2 (nanocatalyst). The nanocatalyst was recovered by centrifugation, washed with DIW, dried on a

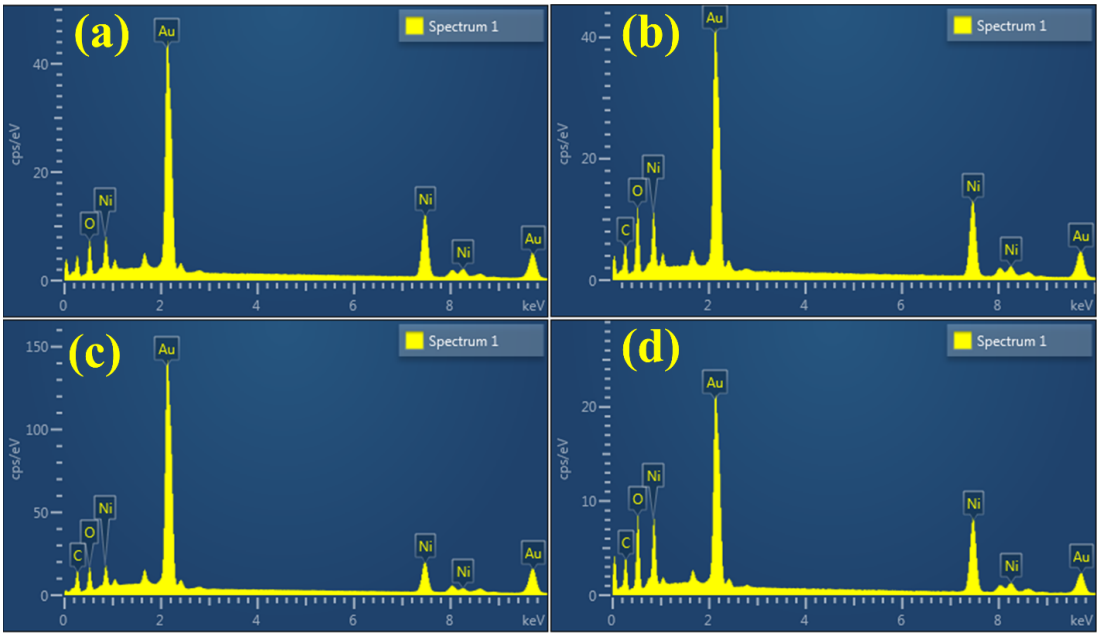

Figure 5. EDS profiles of (a) NiO_2 (b) PEG-doped NiO_2 (c-d) 2 and 4% CS/PEG-NiO_2, respectively.

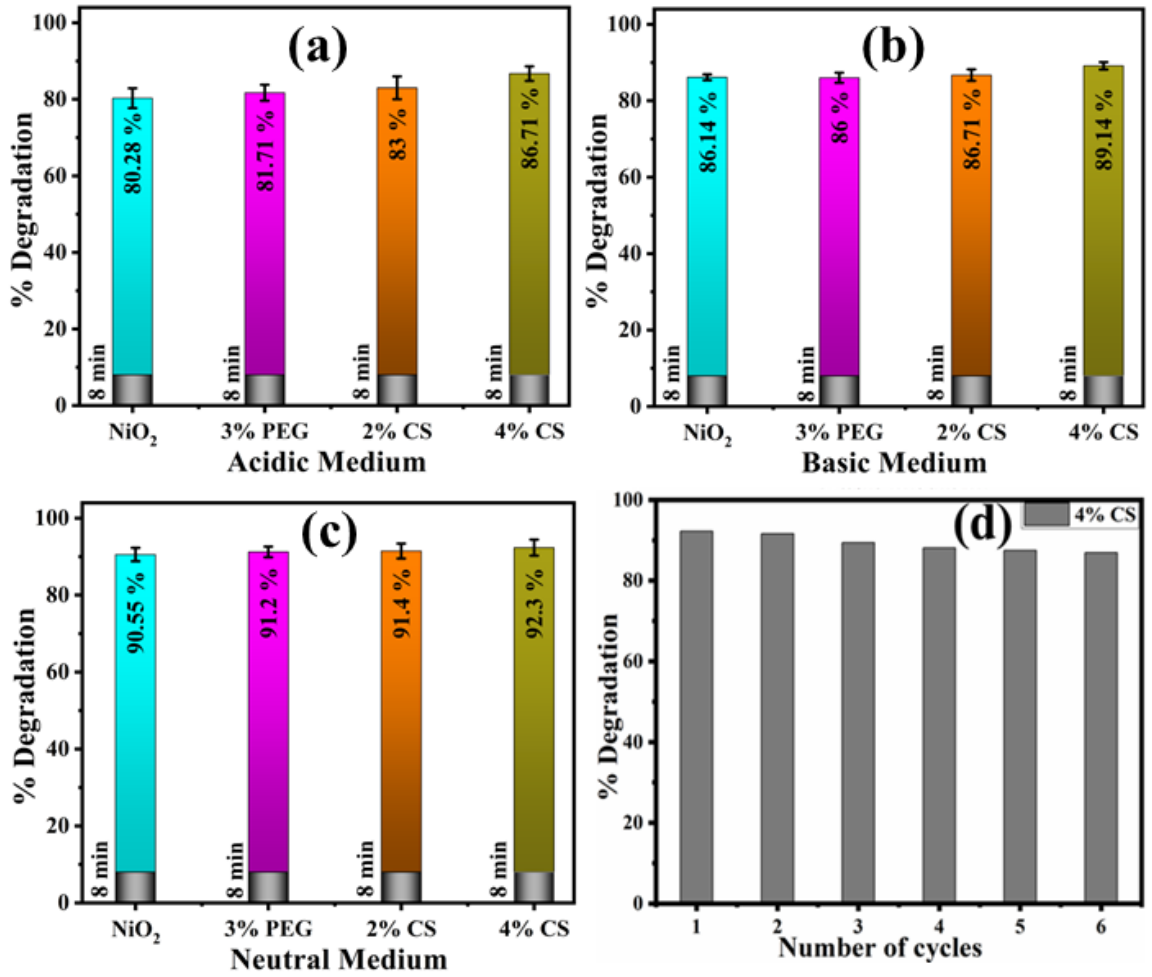

Figure 6. Catalytic dye degradation efficacy of NiO_2 and CS/PEG doped NiO_2 in (a) acidic (pH = 4), (b) basic (pH = 12), and (c) neutral (pH = 7) media respectively within 8 minutes (d) Reusability assay of 4% CS doped sample.

hot plate, and then reused for subsequent cycles. Catalytic degradation (%) efficacy was checked after each cycle, and the obtained results are consolidated in Fig. 6 (d). After the sixth cycle, 91.7% retention of efficacy was observed, inferring a significant recyclability potential of the synthesized nanocatalyst. SEM micrographs of 4% CS/PEG-doped NiO_2 before and after catalysis are presented in Supplementary Fig. 5 (a,b). Micrographs revealed that nanoparticles retain their integrity after dye degradation activity. Comparison table of present work with literature was revealed in Supplementary Table 1.

3.3 Bactericidal activity of synthesized NiO_2

To elucidate the bactericidal behavior of NiO_2, PEG-NiO_2 and (2 and 4%) CS/PEG-doped NiO_2 against MDR *E. coli*, agar well diffusion method (Supplementary Fig. 6 (a,b)) was utilized and measured inhibition zones were quantified

Table 1. Measured inhibition zones (mm) against MDR *E. coli*.

Samples	Inhibition zone (mm) at low concentration (0.5 mg/50 µL)	Inhibition zone (mm) at high concentration (1.0 mg/50 µL)
NiO_2	1.95 ± 0.05	2.75 ± 0.04
3% PEG-NiO_2	2.55 ± 0.04	3.65 ± 0.04
2% CS/PEG-NiO_2	3.65 ± 0.04	4.45 ± 0.03
4% CS/PEG-NiO_2	4.45 ± 0.03	5.25 ± 0.03
Ciprofloxacin	11.15 ± 0.02	11.15 ± 0.02
DI water	0 ± 0.0	0 ± 0.0

and mentioned in Table 1. NiO_2 and CS/PEG-doped NiO_2 displayed inhibition zones 1.95 ± 0.05 - 4.45 ± 0.03 mm and 2.75 ± 0.04 - 5.25 ± 0.03 mm against MDR *E. coli* at minimal and maximal concentrations, respectively. Measured inhibition zones were compared with positive control (ciprofloxacin) and negative control (DI water) possessing inhibition zone values as 11.15 ± 0.02 and 0 ± 0.0 mm respectively. Oxidative stress [51], DNA damage [52], the entrapment of cell with prepared nanocatalysts [53], direct interaction of cell wall membrane with synthesized materials [54] and reactive oxygen species (ROS) [55] all influence bactericidal action. Increased antimicrobial potency was observed in highly doped NiO_2 attributed to the interaction between chitosan and bacterial cells, resulting in cell death.

3.4 Molecular docking analysis

The in-*silico* study offers valuable insights into the structural and functional interactions within ligand-protein systems, thereby deepening our comprehension of the molecular mechanisms that impede the proliferation of bacterial cell membranes. Molecular docking was used to elucidate the mechanism behind antibacterial efficacy of CS/PEG-NiO_2. The cumulative score (cScore) was employed to identify the most favorable ligand conformations within active sites of protein. The docking scores (cScore) for inhibitors NiO_2, PEG-NiO_2, CS/PEG-NiO_2, and Ciprofloxacin, in relation to their binding affinity to 6L01, are noted as 4.12, 4.98, 7.44, and 5.45, respectively. The scores suggest that CS/PEG-NiO_2 establishes most stable complex, demonstrating significant binding affinity for protein. CS/PEG-NiO_2, with its complex structure that includes numerous oxygen atoms, engages in multiple hydrogen bond interactions with adjacent residues across all protein-ligand complexes, thereby significantly enhancing its docking scores. Figure 7 (a) illustrates notable changes in conformation within the complex structure after the energy minimization process. In 6L01-bonded system, NiO_2 interacts with the active site, connecting with residue depicted in Fig. 7 (b). In PEG-NiO_2, it occupies the ligand binding cavity, facilitating optimal interactions such as hydrogen bonds with Gly77, and Ala47, van der Waals interactions with Glu50, Thr165 and Ile78 (Figure 7c,$\acute{c}$). In the CS/PEG-NiO_2 framework (Fig. 7 (d,d$'$)), notable hydrogen bond interactions are observed with Glu50, Thr165, AsP73, which are further augmented by Van der Waals interactions involving Gly77, Ile78, Val165. The interactions observed exhibit resemblance to the standard Ciprofloxacin within DNA gyrase-inhibitor complex (Fig. 7 (e,e$'$)). Figure7 (c$'$-e) illustrates the two-dimensional interaction of the inhibitor-protein complex to improve understanding. The findings clarify the enhanced binding affinity of CS/PEG-NiO_2 for DNA gyrase. The computational results demonstrate a significant alignment with experimental data, providing a strong rationale for the bactericidal effectiveness of CS/PEG-NiO_2 in inhibiting the DNA gyrase of *E. Coli*. This research underscores innovative interdisciplinary methodology that merges experimental antimicrobial assessment with computational docking simulations, thereby offering in-depth insight into the antibacterial mechanisms of CS/PEG-NiO_2. The relationship observed between experimental inhibition zones and molecular docking scores substantiates inhibitory capability of nanostructure in relation to bacterial DNA gyrase. It is significant that elevated cScore associated with CS/PEG-NiO_2 aligns closely with its demonstrated bactericidal activity, illustrating efficacy of computational modeling in predicting and elucidating experimental results. This integration not only deepens our understanding of mechanisms but also facilitates thoughtful design of nanomaterials tailored for specific biological functions.

Current study offered certain limitations about the commercialization of synthesized nanocatalysts against RhB and as an antibiotic for the treatment of bovine mastitis. Present study solely discussed antibacterial effectiveness against gram negative MDR strain, while antibacterial spectrum could be highlighted by employing multiple strains. In future, cytotoxicity assay is encouraged to ensure the biocompatibility and safety of nanostructures.

4. Conclusion

In this study, a cost-effective, low-temperature co-precipitation method was used to synthesize NiO_2 and CS/PEG-doped NiO_2 NSs. Moreover, catalytic and bactericidal activities of the synthesized NSs were examined. The hexagonal structure of NiO_2 was verified through XRD diffraction pattern and no additional peaks were observed with dopants. However, crystallite size decreased from 39.03 to 18.16 nm under the effect of capping agents. SAED analysis confirmed the semicrystalline nature of NiO_2 and 4% CS/PEG-NiO_2. NiO_2 showed more absorption in the visible region and the incorporation of PEG and CS enhanced absorption, leading to an increase in band gap energy values as validated from UV-Vis spectroscopy. Combination of nanoparticles and nanorods was noticed in the TEM image of NiO_2 and the sizes and agglomeration of rod decreased upon dopants. Particle size of the NiO_2 nanostructures decreases from 34.7 to 24.53 nm with the addition of dopants. EDS profiles authorized the presence of doping elements in the host matrix. The highest degradation of RhB dye was witnessed in neutral medium, having an efficacy 92.3% in 8 min for highly doped NiO_2 NSs. Additionally, 4% CS/PEG-doped NiO_2 NSs showed an inhibition zone value 5.25 ± 0.03 mm against gram-negative MDR *E. coli* at high concentration. Computational studies enabled the prediction of molecular interactions and improved the design of nanostructures for antibacterial applications. In conclusion, CS/PEG-doped NiO_2 NSs could be served as efficient RhB dye degrader and bactericidal agent against MDR *E. coli*. Although finding highlights the potential of CS/PEG-NiO_2 in degrading toxic organic pollutants and bactericidal activity against MDR bacterium under controlled conditions. Further investigation is needed to evaluate long term stability, practical applicability and scalability, and this work presents the potential of catalysts for small range of bacterial strain. These limitations clarify the scope of the study and should be considered when interpreting the broader implications of the findings.

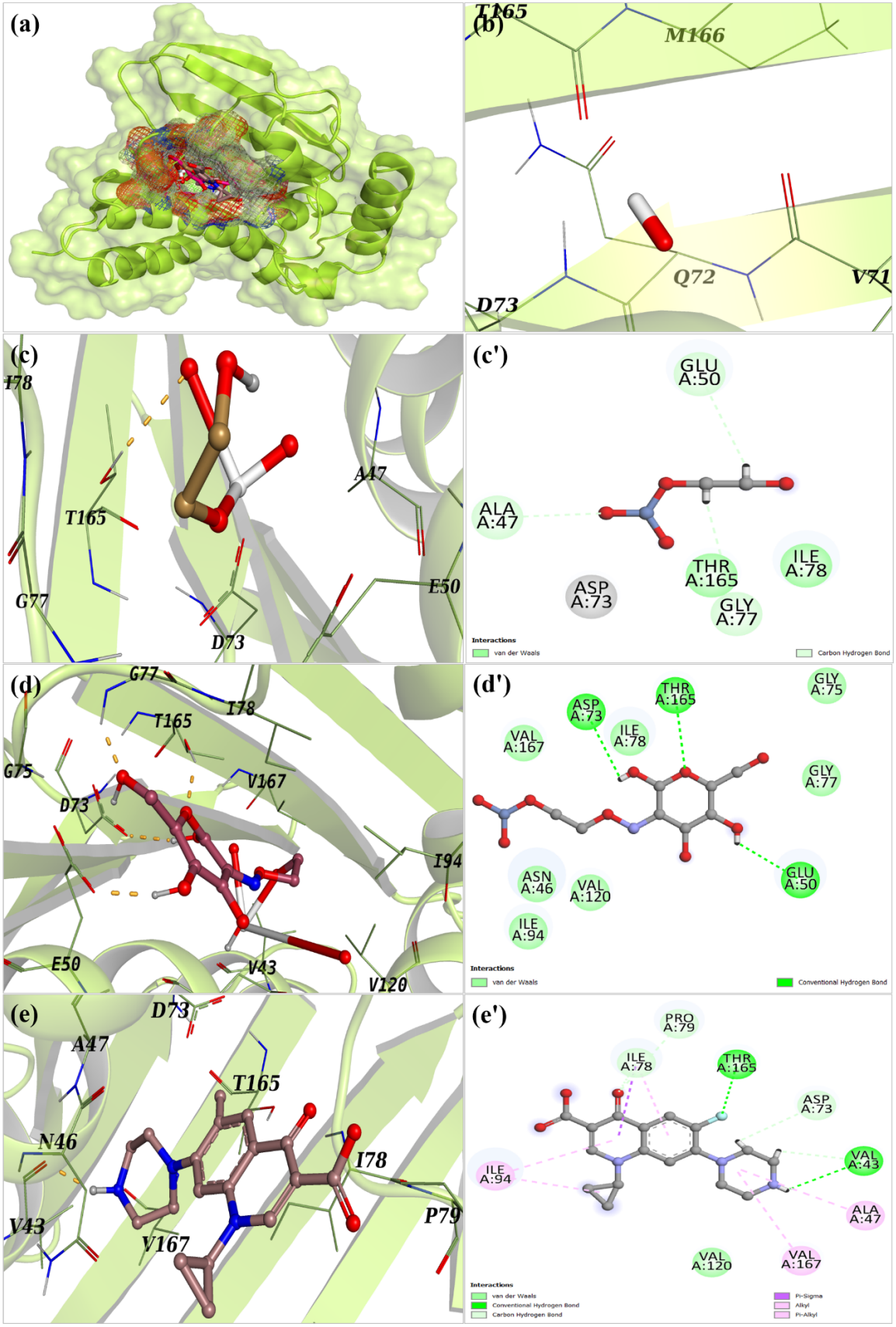

Figure 7. (a) Binding modes of ligands in the binding domain of DNA gyrase, (b) Binding mode of compound NiO_2 in DNA gyrase binding site, (c(3D), c′(2D)) PEG-NiO_2, (d,d′ (3D,2D) CS/PEG-NiO_2, (e(3D), e′(2D)) Ciprofloxacin.

Acknowledgment
Authors are grateful to HEC, through NRPU project 20-17615.

Authors Contribution
Authors have contributed equally in preparing and writing the manuscript.

Availability of data and materials
The datasets generated (or analyzed) during the current study are available from the corresponding author on reasonable request.

Conflict of interests
The authors declare that they have no known competing financial interests or personal relationships that could have appeared to influence the work reported in this paper.

References

[1] P. Li and J. Wu. "Drinking water quality and public health". *Exposure and Health*, **11**(5):73–79, 2019.

[2] G. Baggio, M. Qadir, and V. Smakhtin. "Freshwater availability status across countries for human and ecosystem needs ". Science of the Total Environment:148230, 2021.

[3] M. Sharma, K. Behl, S. Nigam, and M. Joshi. "TiO_2-GO nanocomposite for photocatalysis and environmental applications: A green synthesis approach". *Vacuum*, **156**:434–439, 2018.

[4] S. Chen, J. Zhang, C. Zhang, Q. Yue, Y. Li, and C. Li. "Equilibrium and kinetic studies of methyl orange and methyl violet adsorption on activated carbon derived from Phragmites australis". Desalination (1-3):149–156, 2010.

[5] T. Islam, M.R. Repon, T. Islam, Z. Sarwar, and M.M. Rahman. "Impact of textile dyes on health and ecosystem: a review of structure, causes, and potential solutions". *Environmental Science and Pollution Research*, **30**(4):9207–9242, 2023.

[6] A.A. Al-Gheethi, Q.M. Azhar, P.S. Kumar, A.A. Yusuf, A.K. Al-Buriahi, R.M.S.R. Mohamed, and M.M. Al-Shaibani. "Sustainable approaches for removing Rhodamine B dye using agricultural waste adsorbents: A review". *Chemosphere*, **287**:132080, 2022.

[7] V. Selvaraj, T.S. Karthika, C. Mansiya, and M. Alagar. "An over review on recently developed techniques, mechanisms and intermediate involved in the advanced azo dye degradation for industrial applications". *Journal of Molecular Structure*, **1224**:129195, 2021.

[8] M. Rauf and S.S. Ashraf. "Fundamental principles and application of heterogeneous photocatalytic degradation of dyes in solution". *Chemical Engineering Journal*, **151**(1-3):10–18, 2009.

[9] T.A. Saleh, M. Mustaqeem, and M. Khaled. "Water treatment technologies in removing heavy metal ions from wastewater: A review". *Environmental Nanotechnology, Monitoring & Management*, **17**: 100617, 2022.

[10] Z. Khan, O. Bashir, M.N. Khan, T.A. Khan, and S.A. Al-Thabaiti. "Cationic surfactant assisted morphology of Ag@ Cu, and their catalytic reductive degradation of Rhodamine B". *Journal of Molecular Liquids*, **248**:1096–1108, 2017.

[11] Y. Liu, Q. Lan, S. Sun, and Q. Yang. "Synergistic oxygen vacancy-rich CuO/visible light activation of peroxymonosulfate for degradation of rhodamine B: Fast catalyst synthesis and degradation mechanism". *RSC Advances*, **12**(5):2928–2937, 2022.

[12] R. Tomar, A.A. Abdala, R. Chaudhary, and N. Singh. "Photocatalytic degradation of dyes by nanomaterials". *Materials Today: Proceedings*, **29**:967–973, 2020.

[13] G.A. Varshan and S.K.R. Namasivayam. "A critical review on sustainable formulation of anti-quorum sensing compounds using nanotechnology principles against Candida albicans". *BioNanoScience*, **15**(1):161, 2025.

[14] L.A. Raj, R. Pavithra, and S.K.R. Namasivayam. "Green route synthesis of Highly Stable Zinc Oxide Nanoparticles using Root Extract of Andrographis paniculata and evaluation of their potential activities". *Plant Nano Biology*, page 100162, 2025.

[15] P. Falcaro, R. Ricco, A. Yazdi, I. Imaz, S. Furukawa, D. Maspoch, R. Ameloot, J.D. Evans, and C.J. Doonan. "Application of metal and metal oxide nanoparticles@ MOFs". *Coordination Chemistry Reviews*, **307**:237–254, 2016.

[16] B. Hameeda, A. Mushtaq, M. Saeed, A. Munir, U. Jabeen, and A. Waseem. "Development of Cu-doped NiO nanoscale material as efficient photocatalyst for visible light dye degradation". *Toxin Reviews*, **40**(4):1396–1406, 2021.

[17] M. Alagiri, S. Ponnusamy, and C. Muthamizhchelvan. "Synthesis and characterization of NiO nanoparticles by sol–gel method". *Journal of Materials Science: Materials in Electronics*, **23**:728–732, 2012.

[18] N. Al-Zaqri, K. Umamakeshvari, V. Mohana, A. Muthuvel, and A. Boshaala. "Green synthesis of nickel oxide nanoparticles and its photocatalytic degradation and antibacterial activity". *Journal of Materials Science: Materials in Electronics*, **33**(15):11864–11880, 2022.

[19] S. Prabhu, T.D. Thangadurai, P.V. Bharathy, and P. Kalugasalam. "Synthesis and characterization of nickel oxide nanoparticles using Clitoria ternatea flower extract: Photocatalytic dye degradation under sunlight and antibacterial activity applications". *Results in Chemistry*, **4**:100285, 2022.

[20] R. Ahmad, T. Bedük, S.M. Majhi, and K.N. Salama. "One-step synthesis and decoration of nickel oxide nanosheets with gold nanoparticles by reduction method for hydrazine sensing application". *Sensors and Actuators B: Chemical*, **286**:139–147, 2019.

[21] M. Khan, R. Ahmad, N. Tripathy, A. Khosla, M.I.R. Khan, P. Mishra, M.A. Syed, and W.A. Ansari. "Fabrication of an ultra-sensitive hydrazine sensor based on nano-chips shaped nickel hydroxide modified electrodes". *Microsystem Technologies*, **28**(1):279–286, 2022.

[22] G.T. Anand, R. Nithiyavathi, R. Ramesh, S.J. Sundaram, and K. Kaviyarasu. "Structural and optical properties of nickel oxide nanoparticles: Investigation of antimicrobial applications". *Surfaces and Interfaces*, **18**:100460, 2020.

[23] A.A. Hassan, H. Adil, T. Alyasiri, R. Alsayed, R. Makia, M. Kadhom, H. Salman, and E. Yousif. "Nickel oxide nanoparticles with ginger extract: An environmentally sustainable method for antibacterial applications". *Results in Chemistry*, **9**:101617, 2024.

[24] S. Arshad, M. Imran, A. Haider, A. Shahzadi, H. Saeed, A. Ul-Hamid, M.M. Al-Anazy, E.S. Yousef, and M. Ikram. "Evaluation of Bactericidal Potential and Catalytic Dye Degradation of Yttrium/Graphitic Carbon Nitride Doped Nickel Oxide Nanostructures". *Journal of Inorganic and Organometallic Polymers and Materials*, **34**(5):2017–2029, 2024.

[25] K. Subramanyam, N. Sreelekha, G. Murali, D.A. Reddy, and R. Vijayalakshmi. "Structural, optical and magnetic properties of Cr doped SnO2 nanoparticles stabilized with polyethylene glycol". *Physica B: Condensed Matter*, **454**:86–92, 2014.

[26] S. Priyanka, S.K.R. Namasivayam, J.F. Kennedy, and M. Moovendhan. "Starch-chitosan-Taro mucilage nanocomposite active food packaging film doped with zinc oxide nanoparticles–Fabrication, mechanical properties, anti-bacterial activity and eco toxicity assessment". *International Journal of Biological Macromolecules*, **277**: 134319, 2024.

[27] L. Wang, S. Wang, and J.Z. Bei. "Synthesis and characterization of macroinitiator-amino terminated PEG and poly (γ-benzyl-L-glutamate)-PEO-poly (γ-benzyl-L-glutamate) triblock copolymer". Polymers for Advanced Technologies(10):617–621, 2004.

[28] R. Sowmya, S.K.R. Namasivayam, K.S. Sivasuriyan, and G.A. Varshan. "Anti-cancer potential of chitosan-starch selenium Nanocomposite: Targeting osteoblastoma and insights of molecular docking". Biochemical and Biophysical Research Communications:151853, 2025.

[29] K.S. Sivasuriyan, S.K.R. Namasivayam, S. Rajendran, and A.V.G. Subbulakshmi. "Biocompatible chitosan-starch bio-composite fabricated with Mukia maderaspatana metabolites: Preparation and evaluation for enhanced potential pharmacological activities". *Next Materials*, **8**:100911, 2025.

[30] J. Zhang, Q. Wang, and A. Wang. "Synthesis and characterization of chitosan-g-poly (acrylic acid)/attapulgite superabsorbent composites". *Carbohydrate Polymers*, **68**(2):367–374, 2007.

[31] K. Naseem, E. Abrar, A. Khalid, and M.A. Ismail. "Inorganic nanoparticles as a potential catalyst for the reduction of Rhodamine B dye: A critical review". *Inorganic Chemistry Communications*, **163**:112367, 2024.

[32] H. Li, J. Liao, and T. Zeng. "A facile synthesis of CuO nanowires and nanorods, and their catalytic activity in the oxidative degradation of Rhodamine B with hydrogen peroxide". *Catalysis Communications*, **46**:169–173, 2014.

[33] D.H. Bergey. "Bergey's manual of determinative bacteriology". Lippincott Williams & Wilkins, 1994.

[34] B. Iwalokun, A. Ogunledun, D. Ogbolu, S. Bamiro, and J. Jimi-Omojola. "*in vitro* antimicrobial properties of aqueous garlic extract against multidrug-resistant bacteria and candida species from nigeria". *Journal of Medicinal Food*, **7**(3):327–333, 2004.

[35] A. Haider, M. Ijaz, M. Imran, M. Naz, H. Majeed, J. Khan, M. Ali, and M. Ikram. "Enhanced bactericidal action and dye degradation of spicy roots' extract-incorporated fine-tuned metal oxide nanoparticles". *Applied Nanoscience*, **10**:1095–1104, 2020.

[36] A. Haider, M. Ijaz, S. Ali, J. Haider, M. Imran, H. Majeed, I. Shahzadi, M.M. Ali, J.A. Khan, and M. Ikram. "Green synthesized phytochemically (Zingiber officinale and Allium sativum) reduced nickel oxide nanoparticles confirmed bactericidal and catalytic potential". *Nanoscale Research Letters*, **15**:1–11, 2020.

[37] I. Shahzadi, M. Islam, H. Saeed, A. Haider, A. Shahzadi, J. Haider, N. Ahmed, A. Ul-Hamid, W. Nabgan, and M. Ikram. "Formation of biocompatible MgO/cellulose grafted hydrogel for efficient bactericidal and controlled release of doxorubicin". *International Journal of Biological Macromolecules*, **220**:1277–1286, 2022.

[38] M.F. Mesleh, J.B. Cross, J. Zhang, J. Kahmann, O.A. Andersen, J. Barker, R.K. Cheng, B. Felicetti, M. Wood, and A.T. Hadfield. "Fragment-based discovery of DNA gyrase inhibitors targeting the ATPase subunit of GyrB". *Bioorganic & Medicinal Chemistry Letters*, **26**(4):1314–1318, 2016.

[39] M. Elabbasy, M. Abd El-Kader, A. Ismail, and A. Menazea. "Regulating the function of bismuth (III) oxide nanoparticles scattered in Chitosan/Poly (Vinyl Pyrrolidone) by laser ablation on electrical conductivity characterization and antimicrobial activity". *Journal of Materials Research and Technology*, **10**:1348–1354, 2021.

[40] C. Vidyasagar and Y.A. Naik. "Surfactant (PEG 400) effects on crystallinity of ZnO nanoparticles". *Arabian Journal of Chemistry*, **9**(4):507–510, 2016.

[41] A.A. Elfadl, A.H. Bashal, T.H. Habeeb, M.A. Khalafalla, N.S. Alkayal, and K.D. Khalil. "Preparation, characterization, dielectric properties, and AC conductivity of chitosan stabilized metallic oxides CoO and SrO: Experiments and tight binding calculations". *Polymers*, **15**: 4132, 2023.

[42] A.M. Mahmoud, F.A. Ibrahim, S.A. Shaban, and N.A. Youssef. "Adsorption of heavy metal ion from aqueous solution by nickel oxide nano catalyst prepared by different methods". *Egyptian Journal of Petroleum*, **24**(1):27–35, 2015.

[43] M.I. Din, S. Rehman, Z. Hussain, A. Intisar, E. Ahmed, A. Sharif, T. Hussain, R. Khalid, S. Ameen, and M. Arshad. "Eco friendly synthesis of nickel oxide nanoparticles and its application on pyrolysis of Calotropis procera (AKH) Plant roots". *Journal of Optoelectronic and Biomedical Materials*, **13**(3):119–125, 2021.

[44] X. Xin, Z. Lü, B. Zhou, X. Huang, R. Zhu, X. Sha, Y. Zhang, and W. Su. "Effect of synthesis conditions on the performance of weakly agglomerated nanocrystalline NiO". *Journal of Alloys and Compounds*, **427**(1-2):251–255, 2007.

[45] G. Nabiyouni, A. Barati, and M. Saadat. "Surface adsorption of polyethylene glycol and polyvinyl alcohol with variable molecular weights on zinc oxide nanoparticles". 2011.

[46] M. Anuje, P.N. Pawaskar, V. Khot, A. Sivan, S. Jadhav, J. Meshram, and B. Thombare. "Synthesis, characterization, and cytotoxicity evaluation of polyethylene glycol-coated iron oxide nanoparticles for radiotherapy application". *Journal of Medical Physics*, **46**(3): 154–161, 2021.

[47] A. Sarhan. "Characterization of Chitosan and polyethylene glycol blend film". *Egyptian Journal of Chemistry*, **62**(Special Issue (Part 2)):405–412, 2019.

[48] S. Jana, G. Mondal, B.C. Mitra, P. Bera, B. Chakraborty, A. Mondal, and A. Ghosh. "Facile synthesis of nickel oxide thin films from PVP encapsulated nickel sulfide thin films: an efficient material for electrochemical sensing of glucose, hydrogen peroxide and photodegradation of dye". *New Journal of Chemistry*, **41**(24): 14985–14994, 2017.

[49] M.I. Din, A.G. Nabi, A. Rani, A. Aihetasham, and M. Mukhtar. "Single step green synthesis of stable nickel and nickel oxide nanoparticles from Calotropis gigantea: catalytic and antimicrobial potentials". *Environmental Nanotechnology, Monitoring & Management*, **9**:29–36, 2018.

[50] S.-J. Hong, H.-J. Mun, B.-J. Kim, and Y.-S. Kim. "Characterization of nickel oxide nanoparticles synthesized under low temperature". *Micromachines*, **12**(10):1168, 2021.

[51] S. Liu, T.H. Zeng, M. Hofmann, E. Burcombe, J. Wei, R. Jiang, J. Kong, and Y. Chen. "Antibacterial activity of graphite, graphite oxide, graphene oxide, and reduced graphene oxide: membrane and oxidative stress". *ACS Nano*, **5**(9):6971–6980, 2011.

[52] A. Kumar, A.K. Pandey, S.S. Singh, R. Shanker, and A. Dhawan. "Engineered ZnO and TiO_2 nanoparticles induce oxidative stress and DNA damage leading to reduced viability of *Escherichia coli*". *Free Radical Biology and Medicine*, **41**(10):1872–1881, 2011.

[53] O. Akhavan, E. Ghaderi, and A. Esfandiar. "Wrapping bacteria by graphene nanosheets for isolation from environment, reactivation by sonication, and inactivation by near-infrared irradiation". *Journal of Physical Chemistry B*, **115**(19):6279–6288, 2011.

[54] O. Akhavan and E. Ghaderi. "Toxicity of graphene and graphene oxide nanowalls against bacteria". *ACS Nano*, **4**(10):5731–5736, 2010.

[55] V. Lakshmi Prasanna and R. Vijayaraghavan. "Insight into the mechanism of antibacterial activity of ZnO: Surface defects mediated reactive oxygen species even in the dark". *Langmuir*, **31**(33):9155–9162, 2015.

Supplementary

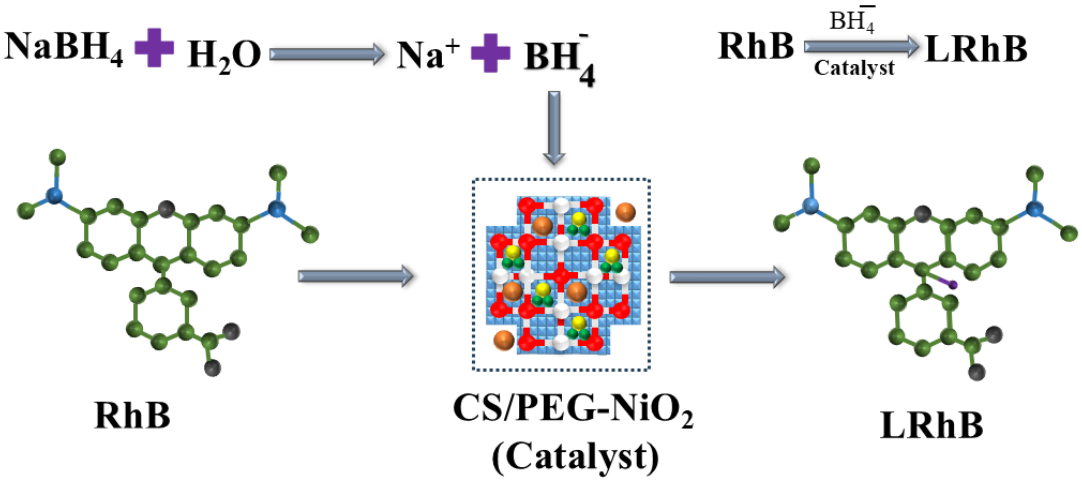

Supplementary Figure 1. Schematic illustration of dye degradation mechanism.

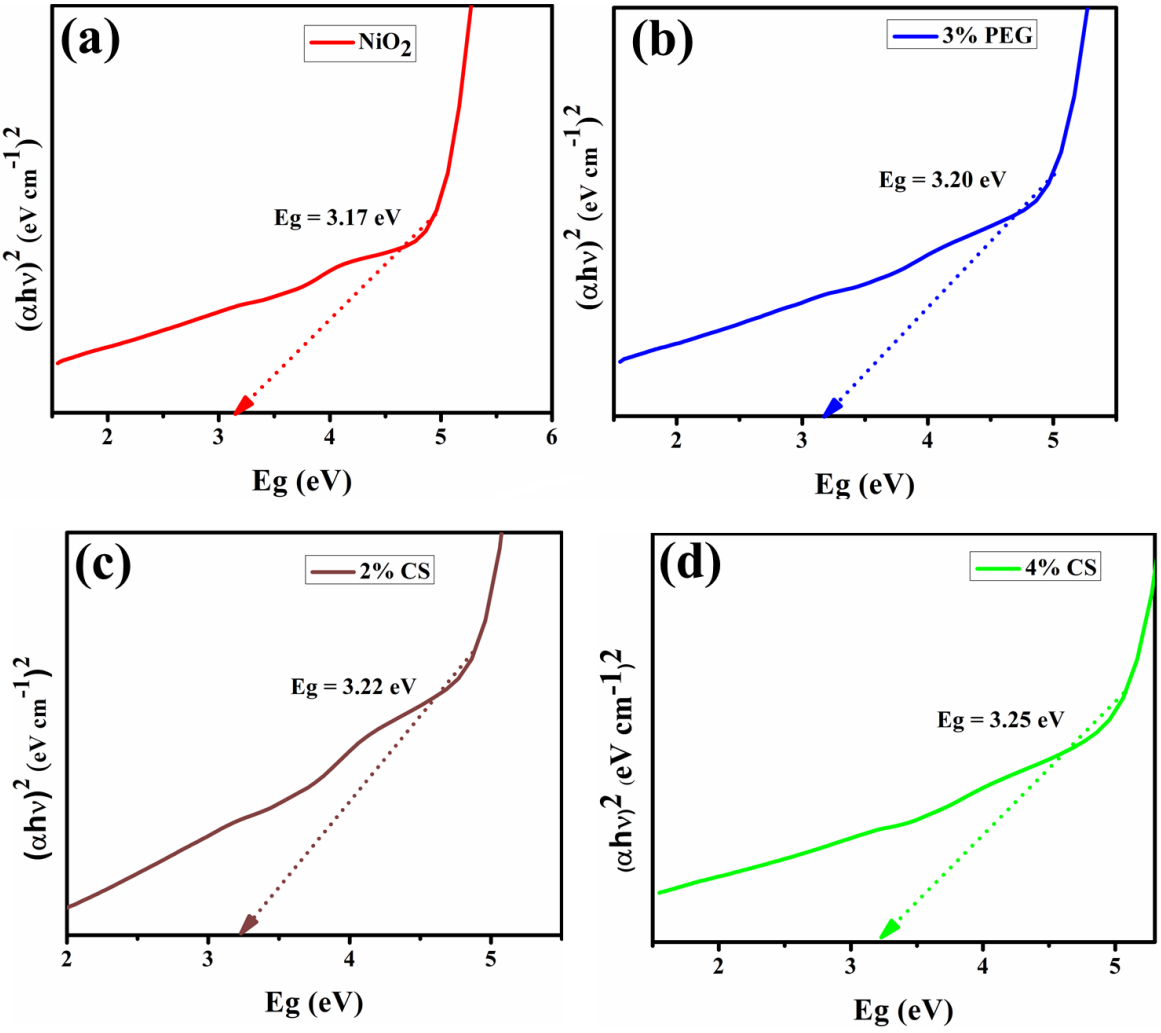

Supplementary Figure 2. Calculated bandgap energy of (a) NiO_2, (b) PEG-dopped NiO_2, (c-d) 2 and 4% CS/PEG-dopped NiO_2.

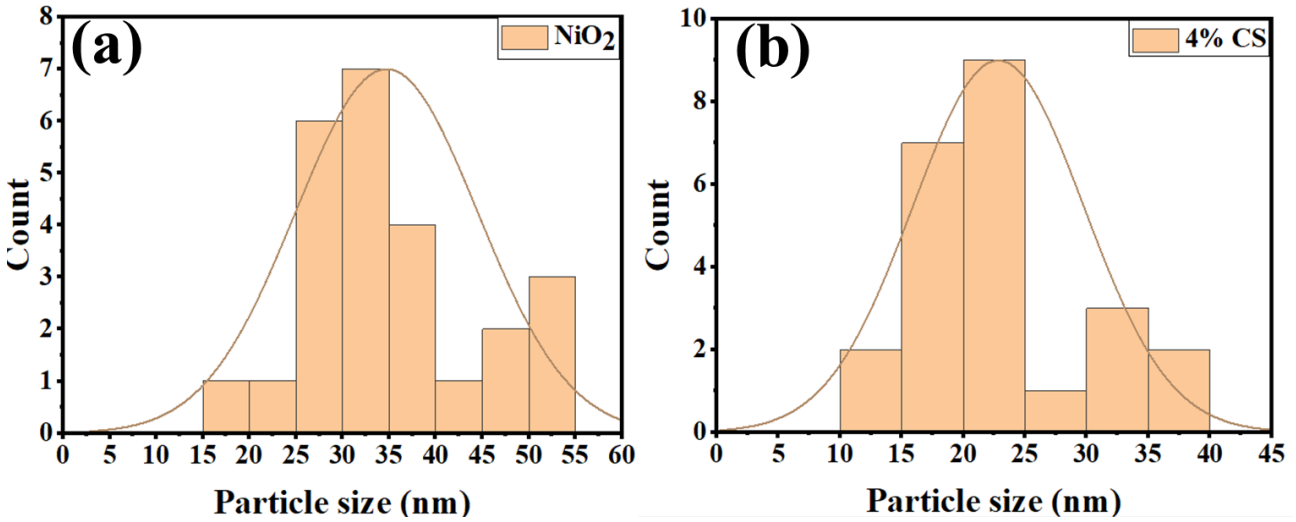

Supplementary Figure 3. Size distribution histograms of (a) NiO_2 and (b) 4% CS/PEG-doped NiO_2.

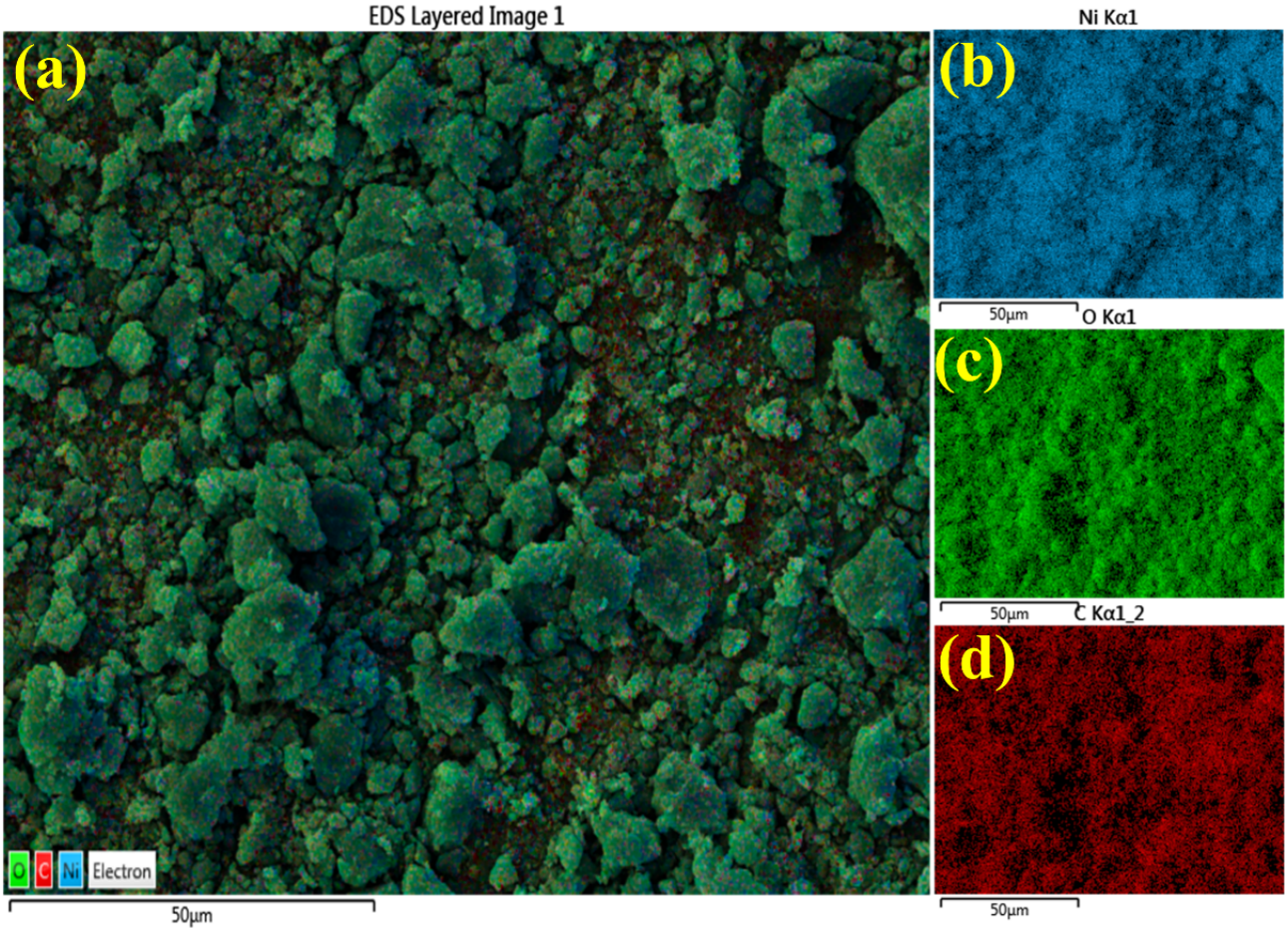

Supplementary Figure 4. Mapping images of 4% CS/PEG-NiO_2.

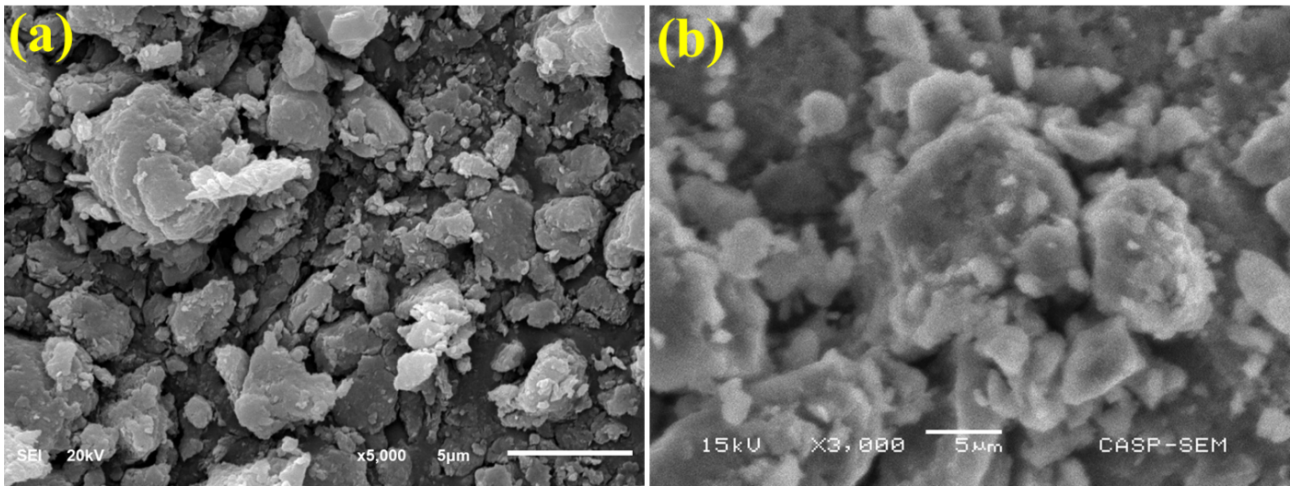

Supplementary Figure 5. SEM micrographs of 4% CS/PEG-doped NiO_2 (a) before catalytic activity against RhB dye and (b) retrieved sample after one cycle of catalysis.

Supplementary Table 1. Comparative analysis of RhB dye degradation efficacy of Ni-based nanostructures.

Samples	Synthesis	% Degradation	Reference
NiO nanoparticles (NPs)	Chemical route	80.33%	https://doi.org/10.1080/16583655.2019.1686248
NiO NPs	Green synthesis	70 – 74%	https://doi.org/10.1134/S1070363224070168
GO-NiO	Green synthesis	79%	https://doi.org/10.1007/s10854-021-07470-5
4% La-doped NiO	Co-precipitation	89%	https://doi.org/10.1016/j.dwt.2024.100731
4% Ag doped NiO_2	Auto-flash-combustion method	90%	https://doi.org/10.1016/j.ijhydene.2024.05.466
NiO/rGO	Hydrothermal	80.2%	https://doi.org/10.1016/j.cplett.2024.141860
4% CS/PEG-NiO_2	Co-precipitation	92.34%	Present study

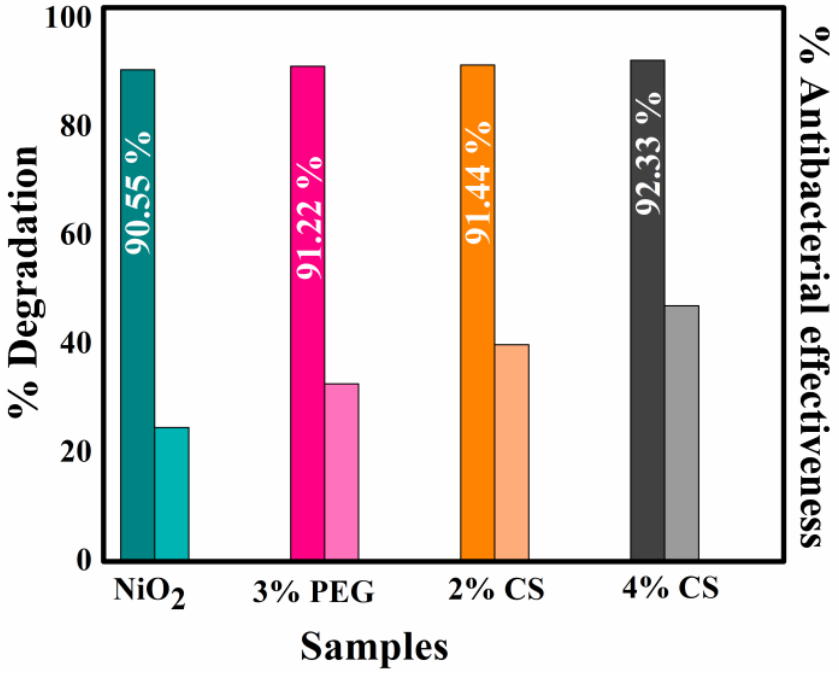

Supplementary Figure 6. Comparative bar chart for catalytic and antibacterial results.

The pseudo-first order model for RhB adsorption can be described as (1)

$$(q_e - q_t) = \log q_e - \frac{k_1}{2.303} t \quad (1)$$

where q_e (RhB concentration at equilibrium) and q_t (RhB concentration after a certain time t) and k_1 is the constant. The pseudo-2nd order model is expressed as (2)

$$\frac{t}{q_t} = \frac{1}{k_t q_{e^2}} + \frac{t}{q_t} \quad (2)$$

For the pseudo-1st order model, the correlation coefficient ($R^2 = 0.81104, 0.78406$) for NiO_2 and highly doped NiO_2, suggesting this model is inappropriate for RhB reduction (Supplementary Fig. 7 (a)). For pseudo 2nd order, the correlation coefficient ($R^2 = 0.9938, 0.99762$) suggesting this model is good for RhB adsorption (Supplementary Fig. 7 (b)).

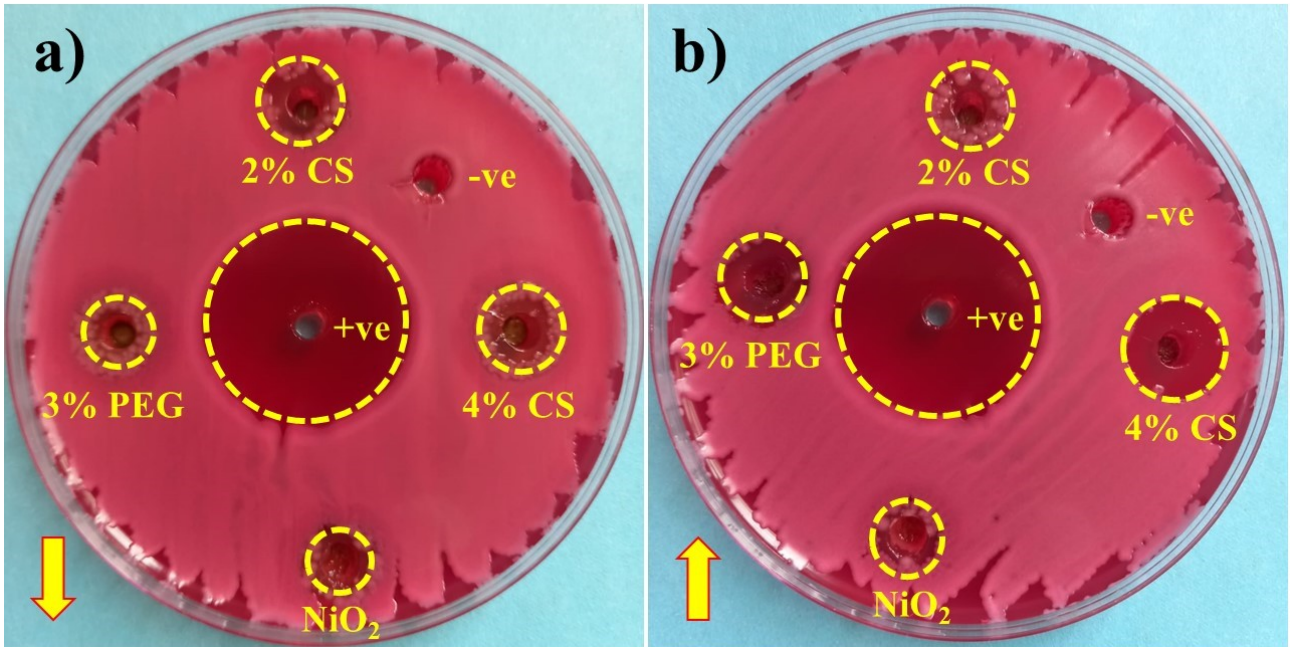

Supplementary Figure 7. *In vitro* bactericidal activity of NiO_2 and doped NiO_2 for MDR *E. coli* at (a) minimal and (b) maximal concentrations.

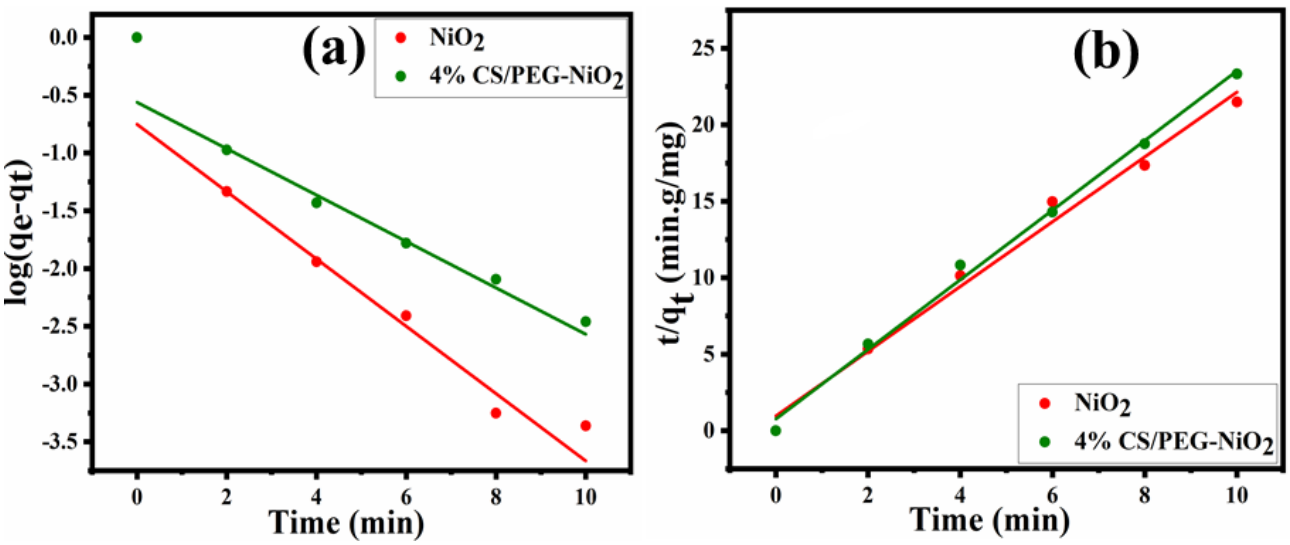

Supplementary Figure 8. (a) Pseudo 1st order and (b) pseudo 2nd order model.

2008-9244[https://doi.org/10.57647/jnsc.2025.1505.20]